Organic Process Research & Development

Article

pubs.acs.org/OPRD

Automated Multitrajectory Method for Reaction Optimization in a Microfluidic System using Online IR Analysis

Jason S. Moore and Klavs F. Jensen*

Department of Chemical Engineering Novartis-MIT Center for Continuous Manufacturing Massachusetts Institute of Technology, 77 Massachusetts Avenue, Cambridge, Massachusetts 02139, United States

Supporting Information

ABSTRACT: An automated multitrajectory optimization platform with continuous online infrared (IR) monitoring is presented. The production rate of a Paal–Knorr reaction is maximized within a constrained temperature and residence time design space. The automated platform utilizes a microreactor system to carry out optimizations with low material requirements and implements a micro IR flow cell for continuous online monitoring of reaction conversion. The approach to steady state at each set of reaction conditions is assessed continuously before the objective function is evaluated and reactor conditions move to the next set point. Several optimization algorithms are tested for their performance on a complex objective terrain. Each function comes to agreement on the optimal conditions but requires a significantly different number of experiments to reach the final conditions. Additionally, multiple objective functions are compared to analyze the trade-off between production rate and conversion.

INTRODUCTION

The optimization of a reaction process is often expensive, requiring significant investments in time and material.[1,2] Microreactor systems carry out these optimizations at reduced costs, due to low material requirements and waste generation.[3,4] Additionally, the reduced channel widths allow for reactions that would be mass transfer limited at larger scales to be kinetically controlled,[5,6] and this enhanced reaction rate often produces significantly higher reaction yields.[7] The use of silicon devices also enhances heat transfer, allowing for tight control of reaction temperature and reducing internal temperature gradients that occur in energetic reactions at larger scales.[8−10] Furthermore, these devices can be operated at high temperature and pressure, allowing access to reaction conditions not achievable in batch.[11,12] These advantages enable a more intrinsic understanding of the reaction under investigation and have found application in a number of industries.[13−15] Moreover, the known fluid-flow characteristics combined with controlled mass and heat transfer effects enable scaling of the optimum conditions to larger production systems.[16,17] Lastly, as these flow experiments are performed sequentially, they can progress towards the optimal conditions using information from previous experiments, so that fewer unnecessary and unproductive experiments are performed that do not show improvement over the current conditions.

In an effort to utilize the advantages of the microscale, our group has recently described a microreactor system to perform single-trajectory automated optimization of reactions in a multivariable design space.[17,18] This optimization platform assessed each reaction once by analyzing a reaction sample by HPLC after a fixed number of residence times. In the trajectory method used, the algorithm was designed to move from an initial condition along a single path toward the optimum. Intelligently updating reaction conditions based on inline analytical techniques has been shown to significantly improve optimization performance.[19] However, in more complex reaction schemes, the terrain of the objective function will not point so directly to the optimal conditions. Herein we describe an expanded multitrajectory optimization system, allowing for the optimization of such a complex reaction system. This analysis takes into account the changing behavior of the objective function by reanalyzing the objective terrain and changing the search direction during the optimization.

This work focuses on the overall approach used to conduct reaction optimizations, regardless of the reaction or the actual objective function. Thus, it would be possible to interchange objectives or even reactions using the same methodology. A well-known method that is often used to accomplish this is design of experiments (DoE); however, this approach assumes that the objective function can be well modeled over its entirety by a low-order function. Here, no such assumption is necessary, and this approach is intended to be extendable to more complex systems where design of experiments would fail to adequately capture the nature of the objective function.

Most previous studies have monitored performance only intermittently and at a single wavelength. In this example, the reaction progression was analyzed quantitatively via online ATR-FTIR using Mettler Toledo's ReactIR microflow cell, which has a 51-μL flow cell equipped with a multipass diamond window to allow for continuous monitoring of the mid-IR range.[20] This analytical technique has previously been used in characterizing system dispersion and chromatographic effects, reaction screening, and monitoring reactor failures, though none of the data was used to quantitatively assess reaction progress, much less investigate reaction kinetics.[21,22] Additionally, use of online IR measurements in process optimization has typically been done by testing a few settings of process

Received: April 16, 2012
Published: July 9, 2012

dx.doi.org/10.1021/op300099x | *Org. Process Res. Dev.* 2012, 16, 1409−1415

variables, changing one at a time, and observing the relative size of the desired peak, without quantitative analysis or investigation of parameter interactions.[23]

The IR microflow cell enables monitoring of the reaction's approach to steady state, ensuring that steady-state data is used for analysis. Thus, the next set of reaction conditions can begin as soon as the previous steady state had been reached and assessed, rather than waiting a fixed number of residence times and assuming that steady state has occurred, as has been done previously.[18] Moreover, this analysis can be performed directly inline at reaction concentrations by using the entire reactor effluent, rather than requiring significant dilution of only a small reaction sample, as with HPLC sampling, enabling better characterization of system fluctuations and nondestructive analysis between unit operations. It would also be possible to monitor the reaction with online IR in the presence of unknown reaction species (intermediates or byproducts); however, as with any measurement technique, each reaction species would have to be isolated and calibrated to be certain of quantitative analysis. In addition, the impact of unknown species is dependent on the spectrum analysis technique used. For calibration to a peak height, other species are less likely to have adverse effect unless they contain an overlapping peak. Conversely, if a chemometric principle component analysis is used, any significant uncalibrated impurity can result in altering the spectrum decomposition, preventing quantification. For these reactions, inline analysis would have to be done with other methods such as HPLC, as has been demonstrated previously.[18]

A Paal–Knorr reaction of 2,5-hexanedione (**1**) and ethanolamine (**2**) in dimethyl sulfoxide (DMSO) (Scheme 1), where

Scheme 1. Paal–Knorr reaction.[32,33]

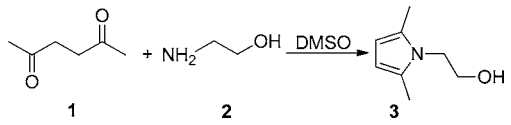

1 2 3

both the first and second reaction steps affect the overall rate, leads to a more complex conversion profile, although the exact structure of the reaction intermediate is still under some debate.[24,25] At short reaction times the initial second-order step significantly affects the overall rate of product formation, which leads to a tapered plateau in the reaction production rate. The Paal–Knorr reaction is widely used to form pyrrole rings in synthetic[26,27] and biological molecules.[28,29] Beyond the mechanism (Scheme 2), the Paal–Knorr reaction has been studied to create libraries[30] and was recently the subject of an optimization and scale-up study.[31] However, more standard one-at-a-time and DoE methods were used to optimize conversion via offline GC analysis after quench and dilution.

While it is possible to determine conversion on the basis of the advanced chemometric analysis of the IR spectrum, reaction conversion of the Paal–Knorr reaction could be monitored simply by calibration to a single peak height normalized to a single point baseline. Figure 1 shows the IR spectrum of the main reaction species, enumerating the main peaks that could be easily followed to assess reaction conversion by monitoring hexanedione consumption and product formation.

Other works have investigated the use of various online analysis techniques to continuously analyze the components of flow systems. For example, Mechtilde et al.[35] have shown that they can use an external Raman probe to scan different residence times down the reactor length. While feedback and optimization are mentioned as possible applications of this technique, no details or results from such are given. The Kazarian group[36] has demonstrated the ability to generate 8 fps IR movies of the entire flow path, which has the potential to be a powerful tool. However, at present this approach still has significant challenges that must be overcome. The small size of the array, approximately a few millimeters on a side, limits the residence times that can be monitored. Also, the use of paraffin walls limits applicable chemistries and temperature range. Furthermore, having the IR detector as the reactor base prevents the decoupling of reactor and measuring temperatures, requiring that calibrations be a function of not only concentration but also temperature.

Herein, we present a microreaction platform and compare the performance of several automated optimization algorithms used to optimize multiple objective functions related to the Paal–Knorr reaction. This setup and these methods aim to target issues of high cost and difficulty typically involved in finding optimal conditions in a complex reaction system.

EXPERIMENTAL SECTION

The microfluidic system used is shown schematically in Figure 2, including a schematic of the silicon microreactor. Flow was achieved with two Harvard syringe pumps (PHD 2000), which were controlled via daisy-chained RS-232 communications to a Dell (Optiplex 960) computer. These syringe pumps were connected to a silicon microreactor with a 232-μL reaction zone and a cooled inlet/outlet zone, which allows the reactant streams to fully mix before reaction occurs and thermally quenches the reaction.[37,38] In addition, due to the high heat transfer coefficient of silicon, the temperature of the reaction zone could be quickly changed between set points and the fluid stream rapidly reached the desired temperature in both reaction and quench zones.

The temperature of the reaction zone was controlled with an Omega (CN9311) controller and an Omega (CSS-01235/120 V) heating cartridge. This controller was connected through an RS-232 cable to the computer to allow programming the temperature set point and reading the measured reactor temperature. The microreactor inlet and outlet region was maintained at room temperature with a recirculating water bath. A Mettler Toledo ReactIR iC 10 outfitted with a DiComp ATR 51-μL flow cell was used for continuous inline monitoring, averaging 167 spectra scans once per minute and saving to an Excel file. The flow cell head was maintained at 35 °C so that spectra were always collected at the same temperature, removing the requirement to account for temperature effects in the IR spectrum. Labview software

Scheme 2. Paal–Knorr reaction mechanism.[25,28,34]

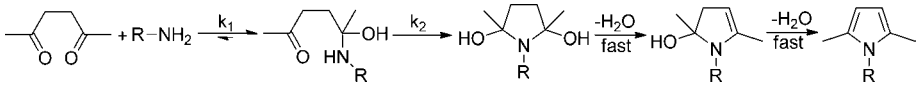

dx.doi.org/10.1021/op300099x | Org. Process Res. Dev. 2012, 16, 1409–1415

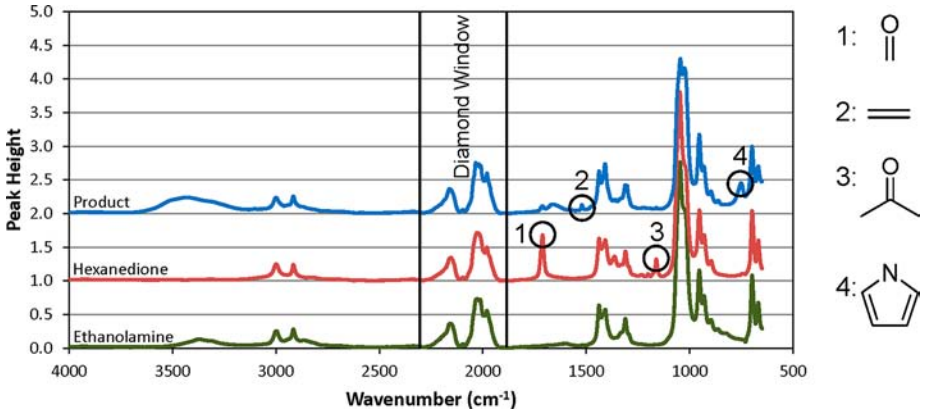

Figure 1. IR spectrum of the Paal–Knorr reaction species and their corresponding moiety in DMSO after solvent subtraction.

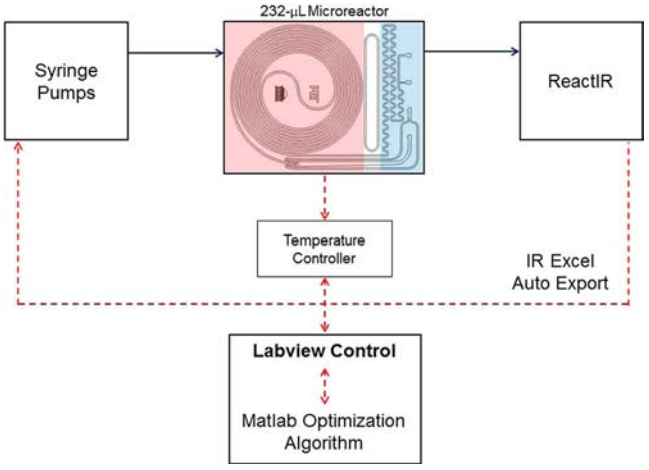

Figure 2. Automation system schematic. Solid lines represent fluid flow and dashed lines represent data flow.

(version 8.5.1) on the computer communicated with the syringe pumps and temperature controller and read the IR Excel export files to determine reaction conversion based on calibrations to peak heights. Matlab scripts (version 2010b) within Labview ran the optimization algorithms to determine reaction set points.

METHOD

Two optimization algorithms, steepest descent and conjugate gradient,[39−41] were used to vary reaction temperature, T, and residence time, τ, to maximize the objective function, J,

$$\max J = \left(\frac{\text{conversion}}{\text{residence time}}\right) = \left(\frac{X}{\tau}\right) \propto \text{production rate} \quad (1)$$

which is proportional to the reaction production rate. The search algorithms were carried out by performing a full-factorial DoE around a starting point, then moving along a trajectory in order to maximize the objective function. The process was then repeated, setting the conditions that maximized the objective function as the new starting point. For the steepest descent algorithm, at each new DoE a new search direction is calculated based solely upon that DoE, which allows the search direction to rapidly change between trajectories. However, for conjugate gradient, the new search direction is a weighted sum of the previous search direction and what would be the new steepest descent search direction. This prevents large shifts in the search direction, which makes the conjugate gradient less likely to become trapped by more difficult terrain.[39]

The optimization was performed by first inputting initial conditions, trajectory and DoE step sizes, and constraints on allowable trajectory conditions. The Matlab optimization algorithm was then started. At each set point, reactor temperature was deemed to be equilibrated once within 1 °C of set point, although the temperature controller generally maintained within 0.2 °C of set point. After equilibration, a minimum flush volume was completed to ensure that the previous steady-state reactor effluent had exited the IR flow cell. The IR data was then continuously monitored until the reaction reached steady state, at which point the objective function was calculated. The algorithm performed an initial DoE around the specified starting location and fit a linear response surface to the objective function. From this surface, the gradient was found and the i^{th} search direction, S_i, was calculated by either the steepest descent (eqs 2a, 2b) or the Fletcher–Reeves conjugate gradient method (eqs 3a–3c).[39] The reaction conditions then stepped along this trajectory until the algorithm either terminated or contracted.

$$S_1 = \nabla J(x_1) \quad (2a)$$

$$S_{k+1} = \nabla J(x_{k+1}), \quad k \geq 1 \quad (2b)$$

$$S_1 = \nabla J(x_1) \quad (3a)$$

$$S_{k+1} = \nabla J(x_{k+1}) + \beta_k S_k, \quad k \geq 1 \quad (3b)$$

$$\beta_k = \frac{\|\nabla J(x_{k+1})\|^2}{\|\nabla J(x_k)\|^2}, \quad k \geq 1 \quad (3c)$$

Termination was triggered if one of the following occurred: (a) by reaching an experimental condition at which all constraints were active, i.e. at a corner of the constrained design space, (b) reaching the maximum number of experiments, (c) reaching a constraint that would cause stepping along the constraint boundary to reduce step size below a set minimum, or (d) when the last objective function calculated was less than or equal to 95% of the maximum objective function value found along the trajectory. This last condition was set at 95% rather than 100% to prevent small decreases in the objective function due to experimental error within relatively flat regions from causing termination.

Contraction was triggered if the objective function decreased with the first step beyond the DoE, indicating that the optimum

dx.doi.org/10.1021/op300099x | Org. Process Res. Dev. 2012, 16, 1409–1415

was very near to the initial condition. Once the trajectory optimum was found, this procedure was then repeated beginning at the trajectory optimum unless contraction occurred and the maximum objective function value found was along the trajectory rather than at a DoE corner within the design space.

The step sizes for the DoE were set to ±2 °C and ±1 min and the trajectory step size was initially set to 3 units (normalized °C and min). These sizes allowed for capturing local variations, which became especially important in the neighborhood of the objective plateau, while allowing for enough change in experimental conditions to have only a small effect due to experimental variances. However, if the trajectory optimum is far from the initial conditions, having a fixed step size on the trajectories can lead to performing experiments at a large number of set points. Thus, an Armijo-type line search[40] was implemented in another optimization run, replacing the previous contraction algorithm. The Armijo algorithm determines the step size, Δx, along the search trajectory by the formula:

$$\Delta x = (-1)^{\beta} \Delta x_{\max} \alpha^{n} \tag{4}$$

Here $\Delta x_{\max}$ is the maximum desired step size, set here to 16 units, and α is a number between 0 and 1, set here to 0.5. While moving along the trajectory, n and β are 0 until a step is not accepted, by triggering a termination criterion. Then Armijo contraction is performed around the current trajectory maximum by setting β to 0 or 1, based upon which interval around the maximum should contain the optimum by the bisection or quadratic interpolation methods, and incrementing the value of n by 1 until the step is accepted or the minimum step size is reached, completing termination.

RESULTS AND DISCUSSION

A Paal–Knorr reaction (Scheme 1) was used to show the performance of this multitrajectory automated optimization platform within the constraints 30 °C ≤ T ≤ 130 °C and 2 min ≤ τ ≤ 30 min on the trajectory points and DoE center points. This maximum temperature was set for the reaction due to the use of a polycarbonate reactor cover. As polycarbonate has a glass transition temperature of 150 °C, a maximum temperature limit was set slightly lower. Along the same lines, a minimum residence time of 2 min was set because a faster pumping rate would cause the system pressure drop to exceed the capabilities of the Harvard syringe pumps. As the overall goal was not simply to show what conditions led to maximizing the objective function, but a total methodology for performing the optimization, constraint handling was deemed relevant, since no real parameter space is without limit. However, as it was possible to replace the polycarbonate cap with pyrex, a further optimization was run to investigate higher temperatures where decomposition and vaporization became issues.

Results for the optimization of the objective function (eq 1) with constant step-size trajectories for the steepest descent and conjugate gradient methods can be seen in a and b in Figure 3, respectively. Additionally, results from the combination of the conjugate gradient and the Armijo algorithms can be seen in Figure 3c. In each figure, values of the objective function are given by the color bar at right, control variable boundaries are denoted by dashed red lines, initial conditions are boxed in black at the bottom left, optimal conditions are boxed in red at the top left, and the initial DoE of each trajectory is numbered.

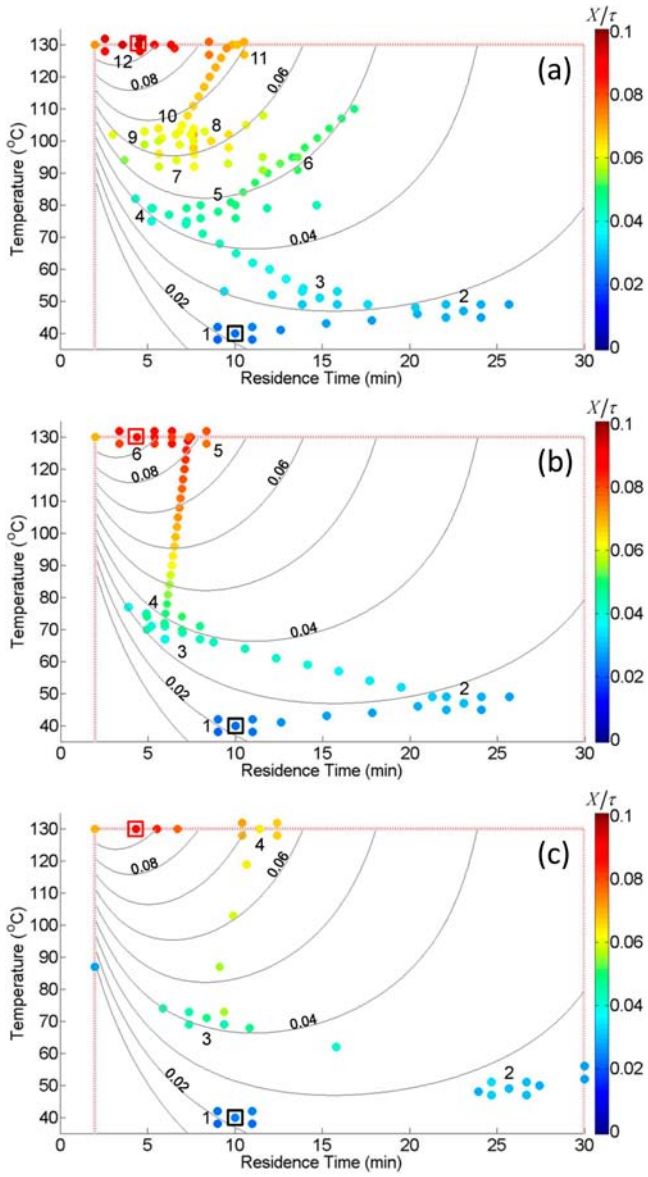

Figure 3. Maximization of the production rate of the Paal–Knorr reaction (Scheme 1) with different optimization strategies. Values of the objective function are given by the color bar at right. Center point control variable boundaries are denoted by dashed red lines. The initial conditions are boxed in black at the bottom left, and the optimum is boxed in red at the top left. The initial DoE of each trajectory is numbered. (a) Steepest descent method. (b) Conjugate gradient method. (c) Armijo conjugate gradient method.

Full tables of conditions, conversion, and objective function values are given in the Supporting Information, in additional to the model used to provide the plot contours. The initial conditions of 40 °C and 10 min residence time can be seen in the box at the lower left in the figures. Both search-direction algorithms initially moved rapidly toward increasing residence time at low temperature. The steepest descent method begins to zigzag (Figure 3a), moving slowly upwards in temperature with large changes in residence time in a low-efficiency manner that is typical of this algorithm type when moving along ridges.[39] This behavior becomes worse in trajectories 4–9 as the sides of the ridge in the objective function become steeper, forcing the trajectories to take only a few steps before moving off the plateau and terminating. Only by happening to have a

dx.doi.org/10.1021/op300099x | Org. Process Res. Dev. 2012, 16, 1409–1415

Table 1. Summary of optimization algorithm performance

method	number of trajectories	number of set points	total volume (mL)	optimum				
				T (°C)	τ (min)	X	X/τ	$J_{penalty}$
Steepest Descent	12	126	44.6	130	4.49	0.420	0.094	0.632
Conjugate Gradient	6	75	25.2	130	4.36	0.385	0.088	0.594
Armijo Conjugate Gradient	4	38	13.9	130	4.36	0.387	0.089	0.597
Penalized Armijo Conjugate Gradient	2	17	6.5	130	12.36	0.807	0.065	0.786
				130	30.00	0.935	0.031	0.754
Optimization Above 130 °C	4	48	17.0	212	6.00	0.764	0.127	0.843

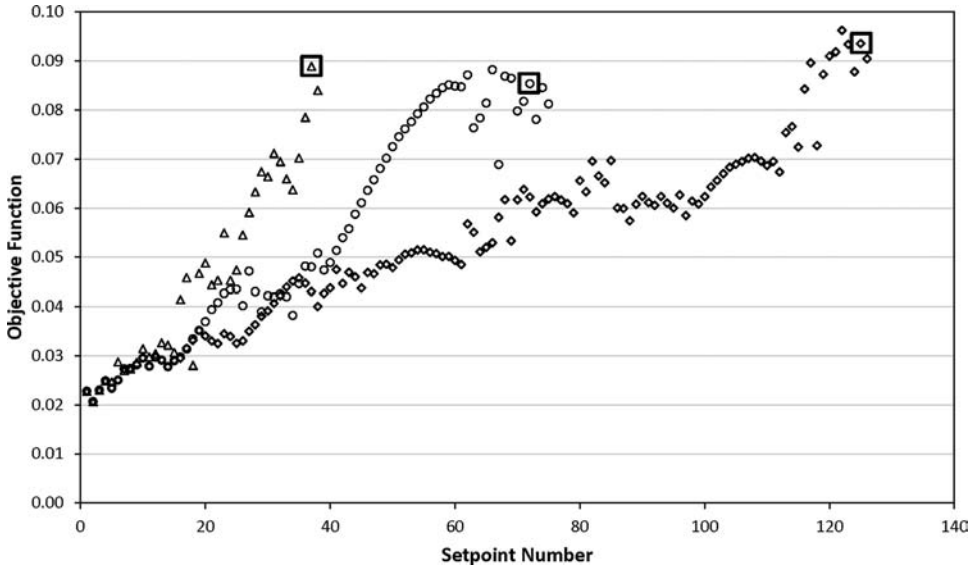

Figure 4. Objective function value at each set point for steepest descent (diamond), conjugate gradient (circle), and Armijo conjugate gradient (triangle). The optimum for each algorithm is boxed.

point near the very center of the plateau at a particular temperature would the trajectory point enough toward increasing temperature to end this pattern. Trajectory 5 nearly accomplished this, but the large number of points beyond the optimum indicates that the objective decreased slightly beyond it, but stayed within 95% for several points before terminating. Had this trajectory been slightly more in the positive temperature direction, as in trajectory 10, it would have significantly decreased the total number of experiments.

The conjugate gradient algorithm approaches the optimum much more efficiently because the algorithm cannot double back upon itself the way that steepest descent can. In Figure 3b, trajectory 2 appears to double back, but compared to Figure 3a, this behavior is much less pronounced. Trajectory 3 is then very short for the same reason, where the gradient of the DoE points largely towards increasing residence time but the algorithm prevents such a large change in the search direction. Trajectory 4 then continues to adjust the search direction, resulting in a search that bypasses the troubles of steepest descent.

The comparison of b and c of Figure 3 reveals that further efficiency gains are realized by the implementation of the Armijo line search, which significantly reduces the number of set points necessary along the trajectories. Additionally, the ability of the Armijo algorithm to find a better trajectory optimum ensures that the search directions of the conjugate gradient more correctly points toward the design space optimum, resulting in fewer trajectories.

Ultimately, all three algorithms contracted along the upper temperature boundary and reached approximately the same optimum: T = 130 °C and τ = 4.49 min for steepest descent, T = 130 °C and τ = 4.36 min for standard conjugate gradient, and T = 130 °C and τ = 4.36 min for Armijo conjugate gradient. However, the Armijo conjugate gradient method converged at a significantly faster rate, requiring only 38 experimental set points (i.e., individual experiments) in four trajectories, while the standard conjugate gradient required 75 set points in six trajectories, still significantly outpacing the steepest descent, which required 126 set points in 12 trajectories.

The performances of the algorithms are summarized in Table 1 and Figure 4. The points toward the end of the plots are the final optimization along the upper temperature constraint. Because the constraints were on the DoE center and trajectory points but not on the DoE factorial points, some of the points in the last two DoE runs for each method were beyond the allowed space. Thus, these points run at higher temperatures show higher conversion and thus higher objective function values than the optimum, but were not valid optimal points.

The above optimizations of production rate resulted, however, in conversions of only approximately 40%. To attempt to find an optimum at a more desirable conversion, another optimization was performed using a new objective function (eq 5) with a quadratic loss function, a standard method to impose soft inequality constraints,[40] to penalize conversions of less than 85%.

$$\max J_{penalty} = \frac{X}{\tau} - (\max(0, 0.85 - X^2)) + 0.85^2 \quad (5)$$

dx.doi.org/10.1021/op300099x | Org. Process Res. Dev. 2012, 16, 1409−1415

This optimization, shown in Figure 5 was performed using the Armijo conjugate gradient algorithm with the optimum

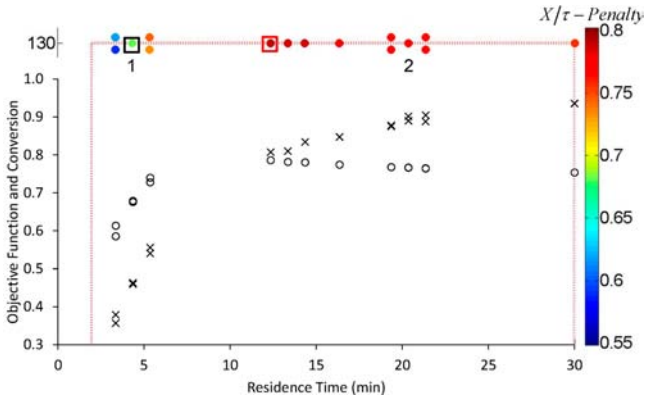

Figure 5. Penalized Armijo conjugate gradient method. The conversion (×) and objective function value (○) at each set point are shown. Values of the objective function are also given by the color bar at right. Center point control variable boundaries are denoted by dashed red lines. The initial conditions are boxed in black at the top left, and the optimum is boxed in red at the top center. The initial DoE of each trajectory is numbered.

from the previous optimization as the initial conditions and ran along the upper temperature boundary of 130 °C. While during the process of the optimization a maximum conversion of 94% was found, the maximum of the penalized objective function was found to be 0.786 at T = 130 °C and τ = 12.36 min, where the conversion was 81% and X/τ was 0.065. Therefore, there is a large trade-off between conversion and production rate. Ultimately, an economic analysis on the full process, including separation costs, would be necessary to determine the desired weighting and limits on the two objectives to use for a final optimization.

As the optimizations performed all found an optimum at which the upper temperature constraint was active, a final optimization was run where the maximum allowable temperature was set only by the ability of the controller to heat the reactor. The results of this optimization utilizing the same penalized objective function with the Armijo conjugate gradient method are given in Figure 6, which found an optimum at 212 °C and 6.00 min residence time with objective value of 0.843, corresponding to a conversion of 76.4%. Here, four trajectories are run with a final DoE around the optimum to confirm that the center point of the DoE has an objective value above that found at the corners. The rapid drop in conversion above 212 °C is due to the vaporization of a large portion of the reaction mixture, causing a transition to annular flow with significantly reduced residence time. This is further compounded by the partial breakdown of DMSO into significantly lower boiling components. While additional backpressure would allow for the reaction to reach somewhat higher temperatures before boiling, the increased DMSO decomposition limits the utility of this approach.

Reaction stoichiometry was not investigated here, because it would result in a trivial optimization where increasing concentration leads to increased reaction rate, as shown by Nieuwland et al.[31] Comparing these two approaches, their approach contained 58 experiments to model the reaction with a resulting leave-one-out cross-validation value of approximately 70%. Here, the final constrained optimization run

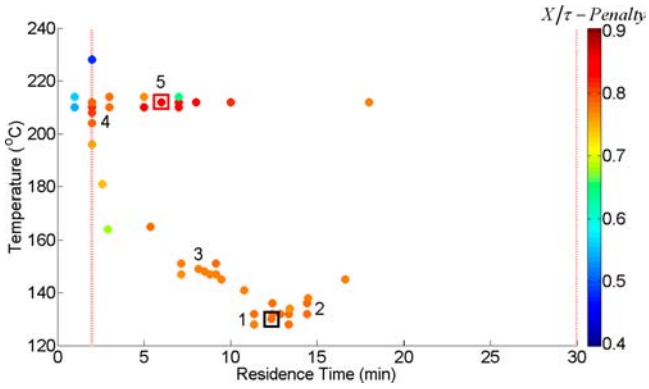

Figure 6. Penalized Armijo conjugate gradient method above 130 °C. Values of the objective function are given by the color bar at right. Center point control variable boundaries are denoted by dashed red lines. The initial conditions are boxed in black at the bottom left, and the optimum is boxed in red at the top left. The initial DoE of each trajectory is numbered.

required only 38 set points to find the optimal production rate and the overall reaction model generated clustered significantly closer to the experimental data (cf. Figure S5, SI).

Because this reaction is relatively well understood, it is known from modeling that the objective is convex within the parameter space, so that regardless of initial conditions, the same optimum will be found. The same initial conditions were used for each search technique to aid in the ability to distinguish their performances. However, for more complex systems, multiple initial conditions may be necessary to test if there are multiple local optima. While global optimization techniques do exist, they tend to require significantly more evaluations of the objective (i.e., experiments) than local search techniques, while still being unable to guarantee that a true global optimum is found.

The above examples demonstrate that the automated system and algorithms can efficiently optimize a range of objectives in a reaction system, including those that offer more complex terrains. The platform is able to perform several sequential experiments with minimal operator intervention. Thus, by intelligently choosing experimental conditions, controlling and monitoring reaction temperature and residence time, and analyzing reactor effluent concentration, not only does the automated microsystem save significant reagents during the optimizations, but also produces significant time savings for the experimenter.

■ CONCLUSIONS

An automated microreactor system combined with continuous online IR analysis has enabled evaluation of multitrajectory optimization strategies for maximizing the production rate of a Pall-Knorr reaction example. The conjugate gradient algorithm was significantly more efficient than the steepest descent method due to the shape of the objective function. Additionally, the incorporation of an Armijo-type line-search algorithm further increased the optimization efficiency. The use of continuous online analysis allowed several measurements of reactor effluent concentrations within a short time, ensuring that each experiment had reached steady state within a set degree of error before moving on to the next set of conditions, allowing for dynamic experiment duration. Thus, each experiment was only as long as necessary, which, paired with

a microreaction system, minimized reagent consumption and further increased system efficiency. Similar techniques could be envisioned for the optimization of more complex reaction systems or those with multiple unit operations, which could incorporate continuous inline IR to nondestructively analyze the output of each step. As there were no significant side reactions, selectivity and impurity profile could not be investigated in this study. However, investigating such aims for other reactions would again simply require interchanging the appropriate objective function to take into account the concentration of one or more side products and to penalize for their formation.

■ ASSOCIATED CONTENT

Supporting Information

Calibrations used for online IR analysis, ^{1}H NMR of the reaction, the conversion and production rate models used, the optimization decision tree, and experimental data. This material is available free of charge via the Internet at http://pubs.acs.org.

■ AUTHOR INFORMATION

Corresponding Author

* E-mail: kfjensen@mit.edu. Fax: 1-617-258-8224. Telephone: 1-617-253-4589.

Notes

The authors declare no competing financial interest.

■ ACKNOWLEDGMENTS

We thank Novartis for financial support and Mettler Toledo for early access to their ReactIR microflow cell and technical assistance.

■ REFERENCES

(1) Geyer, K.; Gustafsson, T.; Seeberger, P. H. *Synlett* **2009**, *15*, 2382−2391.
(2) Jensen, K. F. *MRS Bull.* **2006**, *2*, 101−107.
(3) Kralisch, D.; Kreisel, G. *Chem. Eng. Sci.* **2007**, *62*, 1094−1100.
(4) Hartman, R. L.; Jensen, K. F. *Lab Chip* **2009**, *9*, 2495−2507.
(5) McMullen, J. P.; Jensen, K. F. *Annu. Rev. Anal. Chem.* **2010**, *3*, 19−42.
(6) Hartman, R. L.; McMullen, J. P.; Jensen, K. F. *Angew. Chem., Int. Ed.* **2011**, *50*, 7502−7519.
(7) Hessel, V.; Löwe, H. *Chem. Eng. Technol.* **2005**, *28*, 267−284.
(8) Hessel, V.; Löb, P. In *Micro Process Engineering*; Hessel, V., Renken, A., Schouten, J. C., Yoshida, J.-I., Eds.; Wiley-VCH; New York, 2009; Vol. *1*; pp 367−393.
(9) deMello, A. J. *Nature* **2006**, *442*, 394−402.
(10) Jähnisch, K.; Hessel, V.; Löwe, H.; Baerns, M. *Angew. Chem., Int. Ed.* **2004**, *43*, 406−446.
(11) Marre, S.; Adamo, A.; Basak, S.; Aymonier, C.; Jensen, K. F. *Ind. Eng. Chem. Res.* **2010**, *49*, 11310−11320.
(12) Trachsel, F.; Hutter, C.; von Rohr, P. R. *Chem. Eng. J.* **2008**, *135*, 309−316.
(13) Pennemann, H.; Hessel, V.; Löwe, H. *Chem. Eng. Sci.* **2004**, *59*, 4789−4794.
(14) Schwalbe, T.; Kursawe, A.; Sommer, J. *Chem. Eng. Technol.* **2005**, *28*, 408−419.
(15) Watts, P. *QSAR Comb. Sci.* **2005**, *24*, 701−711.
(16) Wiles, C.; Watts, P. *Adv. Chem. Eng.* **2010**, *38*, 103−194.
(17) McMullen, J. P.; Stone, M. T.; Buchwald, S. L.; Jensen, K. F. *Angew. Chem., Int. Ed.* **2010**, *49*, 7076−7080.
(18) McMullen, J. P.; Jensen, K. F. *Org. Process Res. Dev.* **2010**, *14*, 1169−1176.
(19) Krishnadasan, S.; Brown, R. J. C.; deMello, A. J.; deMello, J. C. *Lab Chip* **2007**, *7*, 1434−1441.
(20) DS Series Sampling Technology. Mettler-Toledo, LLC : Columbus, OH, http://us.mt.com/us/en/home/products/L1_AutochemProducts/L2_in-situSpectrocopy/AgX-FiberConduit-Sampling-Technology-DS-Series.html, Accessed Nov. 7, 2010.
(21) Carter, C. F.; Lange, H.; Ley, S. V.; Baxendale, I. R.; Wittkamp, B.; Goode, J. G.; Gaunt, N. L. *Org. Process Res. Dev.* **2010**, *14*, 393−404.
(22) Brodmann, T.; Koos, P.; Metzger, A.; Knochel, P.; Ley, S. V. *Org. Process Res. Dev.* **2012**, *16*, 1102−1113, DOI: 10.1021/op200275d.
(23) Littler, B. J.; Looker, A. R.; Blythe, T. A. *Org. Process Res. Dev.* **2010**, *14*, 1512−1517.
(24) Amarnath, V.; Anthony, D. C.; Amarnath, K.; Valentine, W. M.; Wetterau, L. A.; Graham, D. G. *J. Org. Chem.* **1991**, *56*, 6924−6931.
(25) Mothana, B.; Boyd, R. J. *J. Mol. Struct.* **2007**, *811*, 97−107.
(26) De, S. *Catal. Lett.* **2008**, *124*, 174−177; , DOI: 10.1007/s10562-008-9461-1.
(27) Li, C.-S.; Tsai, Y.-H.; Lee, W.-C.; Kuo, W.-J. *J. Org. Chem.* **2010**, *75*, 4004−4013.
(28) Li, J.-J., Corey, E. J., Eds. *Name Reactions in Heterocyclic Chemistry*; John Wiley & Sons, Inc.: Hoboken, NJ, 2005.
(29) Balme, G. *Angew. Chem., Int. Ed.* **2004**, *43*, 6238−6241.
(30) Bianchi, I.; Forlani, R.; Minetto, G.; Peretto, I.; Regalia, N.; Taddei, M.; Raveglia, L. F. *J. Comb. Chem.* **2006**, *8*, 491−499.
(31) Nieuwland, P. J.; Segers, R.; Koch, K.; van Hest, J. C. M.; Rutjes, F. P. J. T. *Org. Process Res. Dev.* **2011**, *15*, 783−787.
(32) Knorr, L. *Ber. Dtsch. Chem. Ges* **1885**, *18*, 299−311.
(33) Paal, C. *Ber. Dtsch. Chem. Ges* **1885**, *18*, 367−371.
(34) Amarnath, V.; Amarnath, K.; Valentine, W. M.; Eng, M. A.; Graham, D. G. *Chem. Res. Toxicol.* **1995**, *8*, 234−238.
(35) Mechtilde, S.; Eduard, S.; Andreas, F. *J. Phys. Conf. Ser.* **2006**, *28*, 115.
(36) Chan, K. L. A.; Niu, X.; deMello, A. J.; Kazarian, S. G. *Anal. Chem.* **2011**, *83*, 3606−3609.
(37) Bedore, M. W.; Zaborenko, N.; Jensen, K. F.; Jamison, T. F. *Org. Process Res. Dev.* **2010**, *14*, 432−440.
(38) Zaborenko, N.; Bedore, M. W.; Jamison, T. F.; Jensen, K. F. *Org. Process Res. Dev.* **2011**, *15*, 131−139.
(39) Beers, K. J. *Numerical Methods for Chemical Engineering*; Cambridge University Press: New York, 2007.
(40) Papalambros, P.; Wilde, D. *Principles of Optimal Design*; Cambridge University Press: New York, 2000.
(41) Sun, W.; Yuan, Y.-X. In *Optimization Theory and Methods*; Pardalos, P., Ed.; Springer Science: New York, 2006.